# Strong Metal Support Interaction as a key factor of Au activation in CO oxidation.

**Alexander Yu. Klyushin*[a,b], Travis E. Jones[a], Thomas Lunkenbein[a], Pierre Kube [a], Xuan Li[a], Michael Hävecker[c], Axel Knop-Gericke[a] and Robert Schlögl[a,b,c]**

**Abstract:** We address the question of the nature of Au NP activation and through a combination of experimental and theoretical techniques. In-situ XPS measurements of $Au/TiO_2$ during CO oxidation show high catalytic activity can be associated with the formation of an ionic Au species. DFT calculations performed on $Au/TiO_2$ show that the formation of such ionic Au is due to a strong metal-support interaction between Au and reduced and defective $TiO_2$. TEM supports these findings, indicating the formation of an overlayer of transition metal oxide support on Au NPs after CO oxidation. These results suggest $TiO_2$ lattice oxygen is involved directly in CO oxidation, which was confirmed with labeled $^{18}O_2$ experiments.

The ability of supported gold nanoparticles (Au NPs) to catalyze CO oxidation was discovered by Haruta et al. [1]. Despite considerable attention from the scientific community the reaction mechanism and active sites are still controversial due to the intricate relationships between the structure and function of multiple types of adsorbates (CO, $O_2$, O, OH, $CO_2$) [2,3]. The oxidation state of catalytically active Au is under debate. It was shown that under ultrahigh vacuum conditions or under low oxygen chemical potential anionic Au is formed [4]. On the other hand under catalytically relevant conditions cationic Au species are present [5]. The mechanism proposed for Au on non-reducible supports is based on a reaction between $O_2$, which absorbs on metallic Au, and CO, which adsorbs on cationic Au [3a]. For a model catalyst Goodman proposed a Au activation mechanism via quantum size effect, because small bidimensional Au NPs lose metallic properties [3b]. Finally, two mechanism of CO oxidation on Au involve reducible oxide supports. Haruta proposed that the reaction takes place at the interface between metallic Au NPs and the oxide support, in other words CO adsorbs on Au NPs and the support activates $O_2$ [3c]. Later, a rather similar mechanism was proposed by Bond and Thompsons [3d], they assumed that Au cations at the Au-support interface are involved in the reaction mechanism. To unravel these links we studied $Au/TiO_2$ catalysts using near ambient pressure X-ray photoelectron spectroscopy (NAP-XPS) combined with mass-spectrometry, transmission electron microscopy (TEM), and density functional theory (DFT) calculations.

Our previous work shows that oxygen-free supports do not provide Au NPs that are active in CO oxidation, regardless of particle size and method of synthesis [6]. In contrast, Au NPs on oxygen containing supports show high catalytic activity, which depends on the method of preparation: samples synthesized by deposition-precipitation show significant CO conversion at low temperature, in contrast to photo-induced decomposition method [7]. In this communication we report on the origin of the catalytic activity of Au supported on the transition metal oxide $TiO_2$.

$Au/TiO_2$, obtained by deposition-precipitation [7], was placed in a NAP-XPS chamber to characterize the electronic structure of the fresh catalyst [8]. XP spectra of untreated $Au/TiO_2$ are presented in Figure 1(i). A photon energy of 720 eV was used to collect the Au 4f spectra (Figure 1A), the probing depth was 1.1nm [9]. The Au 4f spectrum of $Au/TiO_2$ before CO oxidation (Figure 1A(i)) shows the presence of two Au species: the main component has a binding energy (BE) of 84.0 eV and is assigned to metallic Au ($Au_{metal}$) [10]; a second component is shifted by 0.6 eV to higher BE and, according to the shift, is assigned to ionic Au ($Au_{ion}$) [3d,10a].

The Au 4f spectrum of $Au/TiO_2$ changes significantly under different gas atmosphere. Under $O_2$, instead of an asymmetric peak consisting of $Au_{metal}$ and $Au_{ion}$, a low intensity symmetric peak appears at BE 84.0 eV (Figure 1A(ii)). Curiously then, the $Au_{ion}$ peak disappears completely under an oxidizing atmosphere, $O_2$ at room temperature. It should be noted that during CO oxidation the catalyst was slightly charging, therefore the provided spectrum was measured in UHV after CO oxidation. However, an asymmetric line shape is restored after CO oxidation in a 1:2 mixture of $CO:O_2$ (Figure 1(iii)). In this case both metallic and ionic components are present in the spectrum, showing the introducing of a reducing agent to the atmosphere results in the apparent oxidation of Au though the intensity of spectrum is almost two times lower than prior to $O_2$ treatment due to carbon accumulation (SI, Figure S3). After CO oxidation, the Au 4f spectrum shows the presence of both the $Au_{metal}$ and $Au_{ion}$ species. The presence of a mixture of $Au^0$ and $Au^+$ was earlier observed under a mixture of CO and $O_2$ using in-situ X-ray absorption (XAS) [11]. The amount of $Au_{ion}$ is larger after reaction than before (the $Au_{ion}/Au_{metal}$ ratio changes from 0.15 to 0.25 before and after CO oxidation, respectively), as shown in Figure 1(iii). This increase in the $Au_{ion}/Au_{metal}$ ratio confirms that $Au_{ion}$ is produced during CO oxidation. Thus, $Au_{ion}$ may play an important role in the reaction mechanism.

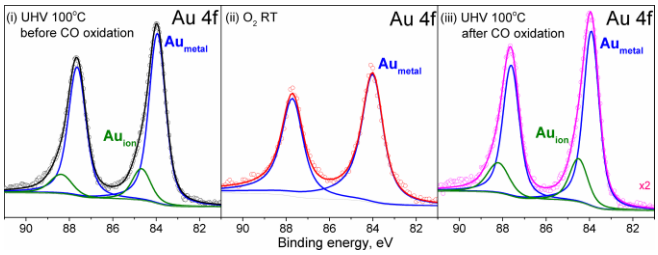


**Figure 1.** Au 4f XP spectra of $Au/TiO_2$ synthesized by deposition-precipitation method (i) in UHV before CO oxidation at 100 °C, (ii) in $O_2$ at room temperature and 0.3 mbar under flow and (iii) in UHV after CO oxidation ($CO:O_2$=1:2) at 100 °C at 0.3 mbar under flow.

To shed light on the origin of the changes in the Au 4f spectra we turned to theory. DFT calculations show that oxidized $TiO_2$ and Au interact weakly, resulting in a calculated or work of adhesion ($W_\infty$) < 0.1 J/m$^2$ (Figure 2A). This is despite the fact that, as previously noted [12], the oxidized interface is the thermodynamically lowest energy state under a wide range of oxygen chemical potentials, see Figure S7. The high stability of the fully oxidized interface is a consequence of the strong Ti-O interaction, allowing Au to remain metallic with a 0.0 eV Au 4f surface core-level shift

[a] Department of Inorganic Chemistry
Fritz Haber Institute of the Max Planck Society,
Faradayweg 4-6, 14195, Berlin, Germany
klyushin@fhi-berlin.mpg.de
[b] Division of Energy Material,
Helmholtz-Zentrum Berlin für Materialien und Energie GmbH
Albert-Einstein-Str. 15, 12489 Berlin, Germany.
[c] Department of Heterogeneous Reactions,
Max-Planck-Institute for Chemical Energy Conversion,
Stiftstrasse 34 – 36, 45470 Mülheim an der Ruhr, Germany.

Supporting information for this article is given via a link at the end of the document

computed for the interfacial Au atoms. In contrast, reduced $TiO_2$ shows a strong metal-support interaction (SMSI), increasing $W_\infty$ to 1.0 J/m$^2$ (Figure 2B). While it is thermodynamically less stable than the oxidized $TiO_2$/Au interface under the oxygen chemical potentials used in our experiments, see Figure S7, the adhesion between Au and support is comparable to the 0.9 J/m$^2$ computed for the Au(110) surface energy. This SMSI is also seen between Au and defective supports (Figure 2C).

Inspection of Löwdin charges suggests the SMSI is due to a depletion of d electrons on the Au atoms at the reduced interface. This reduction in d count leads to Au 4f shifts increasing from 0.0 eV to 0.2 eV, and 0.7 eV for oxidized, reduced, and defected $TiO_2$, respectively. The calculated shifts are in agreement with experimental XPS data (Figure 1A). Furthermore, we did not identify a positive Au 4f shift in other Au/O systems (see SI), suggesting the interaction between Au and the reduced $TiO_2$ surface is responsible for the formation of ionic Au observed in the measured spectra. The XPS results and our calculations suggest that consumption of interfacial oxygen during CO oxidation leads to a SMSI, which traps the system in a meta-stable state where Au is strongly bound to the reduced defective oxide like that modeled in Figure 2C (see SI for more details), giving rise to the ionic Au seen in XPS after CO oxidation.

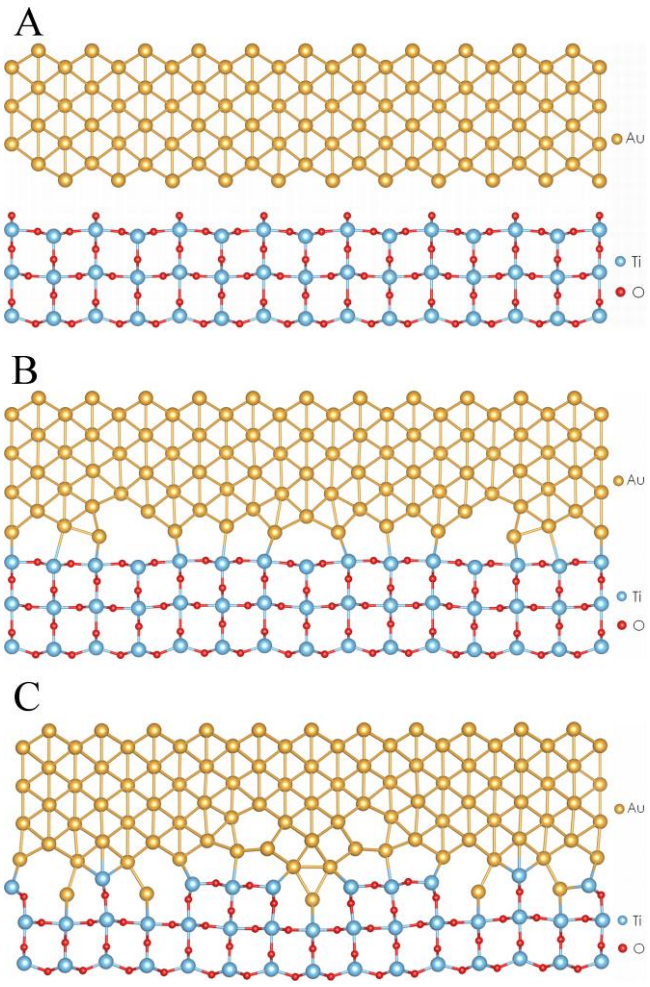


**Figure 2.** Schematic description of the interaction between Au and (A) oxidized, (B) reduced and (C) defective $TiO_2$ (golden balls: Au atoms, red balls: O atoms, blue balls: Ti atoms). A calculated work of adhesion is < 0.1 J/m$^2$ and 1.0 J/m$^2$ for oxidized and reduced $TiO_2$, respectively. High binding energy shifts of ionic Au species are 0.0 eV to 0.2 eV, and 0.7 eV for oxidized, reduced, and defected $TiO_2$, respective

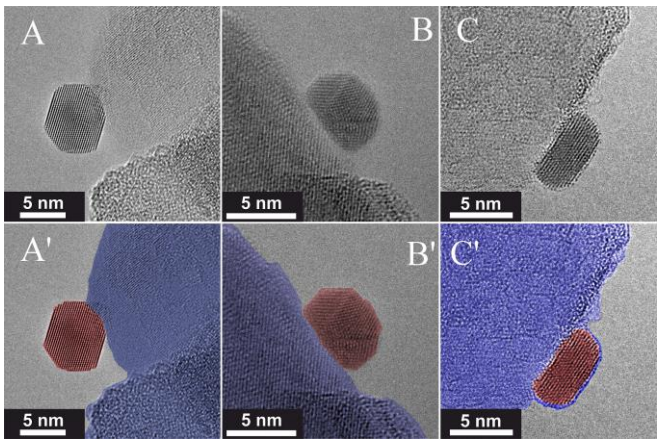


**Figure 3.** TEM images of Au/$TiO_2$ (A) before CO oxidation, (B) after oxidation in $O_2$ at 0.3 mbar and room temperature and (C) CO oxidation (CO:$O_2$=1:2) at 0.3 mbar and 100 °C. At bottom panel the images were colorized in order to highlight the differences between $TiO_2$ support (blue) and Au NP (red).

In order to check this morphological interpretation of the XPS data we turn to TEM to correlate the electronic structure with atomic arrangement. A TEM image of the Au/$TiO_2$ after synthesis is shown in Figure 3A. The Au NPs synthesized by deposition precipitation have a mean diameter of approximately 5 nm before CO oxidation. No overgrowth of the support onto the NPs is visible, and the initial $Au_{ion}$ species are only expected at the contact area between Au and $TiO_2$ after synthesis. Furthermore, after oxidation in $O_2$ TEM does not reveal any changes in size of Au NPs, only the wetting and faceting are different, no spreading of the support material over the Au NP surface was observed (Figure 3B), in agreement with the weak MSI predicted by DFT for oxidized $TiO_2$ and the lack of ionic Au seen in XPS (SI, Table 1S). In contrast, after CO oxidation (CO:$O_2$=1:2) at 0.3 mbar and 100 °C the Au NPs were covered by a thin layer of support material (blue in Figure 3C), which explains a decrease of Au 4f spectrum after CO oxidation. Also these observations confirm the XPS and DFT data, suggesting that SMSI takes place due to the reduction of the Au/oxide interface.

Our present findings explain changes in XP spectra of initially cationic species that are formed at the interface of Au particles and a transition metal oxide by the strong interaction between Au and the oxide. When the surface of $TiO_2$ is fully oxidized DFT predicts that the lack of interaction between Au and oxidized $TiO_2$ will lead to the disappearance of any $Au_{ion}$ in the XP spectrum, which explains the loss of $Au_{ion}$ under an oxygen atmosphere seen in Figure 1. After CO oxidation the $Au_{ion}$ component is present in the XP spectra again due to the reduction of the Au-$TiO_2$ interface by CO, which results in a SMSI. This strong interaction leads to the formation of an oxide overgrowth layer and the metastable structures observed in TEM. This behavior can be explained by removing oxygen atoms from the metal-support border, meaning that lattice oxygen from the transition metal oxide is involved in CO oxidation, this observation is in a good agreement with previous work [3d,13] and suggests CO is oxidized through a Au-assisted Mars–van Krevelen mechanism [13].

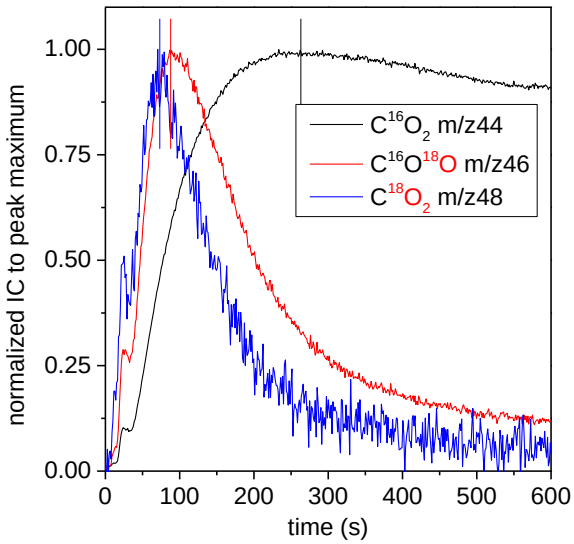


**Figure 4.** Mass-spectrometer signal during CO oxidation with $^{16}O_2$ after saturation of the catalyst with labelled oxygen (via a Mars–van Krevelen like mechanism during CO oxidation with $^{18}O_2$) at 1 bar and room temperature.

Table 1. Catalytic activity of $Au/TiO_2$ catalysts.

| Preparation methods | Metal loading (wt.%) | Diameter of Au (nm) | Rate at 300K (mol $g_{cat}^{-1}$ $s^{-1}$) | $E_a$ (kJ/mol) | Ref. |
|---|---|---|---|---|---|
| Deposition-precipitation | 1 | 4.8 | $4.8*10^{-6}$ | 28.2 | This work,10 |
| Deposition-precipitation | 0.7 | 3.1 | $6.9*10^{-7}$ | 19 | 14a |
| Deposition-precipitation | 1.8 | 2.7 | $5.5*10^{-6}$ | 18 | 14a |
| Impregnation | 1.0 | 10< | $1.7*10^{-10}$ | 58 | 14a |
| Photochemical deposition | 1.0 | 4.6 | $1.5*10^{-10}$ | 56 | 14a |
| Deposition-precipitation | 3 | 4.0 | $1.1*10^{-6}$ | - | 14b |

In order to prove that an a such Mars–van Krevelen type mechanism is relevant, CO oxidation with labeled $^{18}O_2$ was performed at 1 bar. According to our test there is no pressure gap between XPS cell and reactor, under both conditions the catalysts show similar behavior [7]. The sample was mounted in a U-shape plug-flow reactor and treated in $^{16}O_2$ for 30 min at 25°C. After that, CO oxidation with labelled $^{18}O_2$ was performed, which, if the reaction occurs via a Mars–van Krevelen mechanism, will saturate the lattice with $^{18}O$ labeled lattice oxygen (not shown). After this step the reactor was flashed with He and CO oxidation with non-labelled $^{16}O_2$ was performed. Mass-spectrometry shows the formation of $C^{18}O_2$ and $C^{16}O^{18}O$ and later to $C^{16}O_2$ and a fast decrease of the former two signals with time (Figure 4). The obtained results indicate that the lattice oxygen of $TiO_2$ participates in the reaction pathway, which may lead to the formation of locally reduced $TiO_2$ in the vicinity of Au NPs. These observations confirm that the CO oxidation on $Au/TiO_x$ is based on an Au-assisted Mars–van Krevelen mechanism. Despite the relatively large size of the Au NPs, our sample show a high $CO_2$ production rate (Table 1). From Table 1 it is clear that the catalytic performance of the NPs depends on the synthesis method, deposition-precipitation provides more active catalysts, probably because both, metallic and ionic, Au sites are present on the surface after synthesis.

SMSI phenomenon on reduced $TiO_2$ was experimentally observed for the first time almost forty years ago [15]. Cha and Parravano were one of the first who experimentally showed the importance of SMSI effect on $Au/TiO_2$ [16]. Our findings are in the line with the general conclusions about SMSI reached earlier: 1) strong bonding occurs between the metal and reduced support; 2) the metal and the supports interact via charge transferring; 3) SMSI effects are reversed under oxidation conditions [17]. The observed core level XPS shifts match well with Chusuei's work, where they studied the BE of Au clusters on $TiO_2$ as a function of the size of the NPs [18]. The shift was 0.8 eV for Au NPs of 2 nm and decreased with particle size. However, the origin of the BE shifts of metal NPs is controversial, some authors interpret it as an initial-state effect [19], while others attribute it to final state relaxation process [20]. The BE shifts are most likely a combination of both effects. In our case, however, the high BE component is the $Au_{ion}$ bound to reduced $TiO_2$, which is in agreement with recent electron paramagnetic resonance (EPR) experiments that showed a significant amount of $Ti^{3+}$ ions in the vicinity of Au NPs after exposure to CO atmosphere at 120°C [21], where the removal and replacement of $TiO_2$ surface lattice oxygen is reversible under oxidation/reduction conditions. It was shown that CO oxidation is occurring via reaction with lattice O from titanium oxide and that not only the gold surface is involved but rather the gold-oxide interface. Similar conclusions were found by other authors, a Mars–van Krevelen like mechanism has been experimentally observed on $Au/TiO_2$ and takes place at the interface [13,21,22]. Theoretical studies confirm a reaction pathways via a Mars–van Krevelen mechanism at the periphery of titania supported Au NPs [23]. Recently the participation of lattice oxygen in the oxidation of carbon monoxide over Au catalyst supported on cerium oxide was experimentally observed as well [24]. Also it was shown that the presence of reduced $TiO_2$ species for the active catalyst compared to a deactivated catalyst plays the critical role in the wetting of $TiO_2$ by Au [25]. Our isotope label CO oxidation experiments confirm the proposed assumption that $TiO_2$ surface lattice oxygen represents the active oxygen species for CO oxidation at and above room temperature. Our results demonstrate that the nature of the metal/oxide bond is a key factor for Au activation, in particular, the important role of SMSI in the activation of Au-based catalysts.

## Experimental Section

The in-situ XPS measurements were performed at the ISISS beamline of the BESSY II synchrotron radiation facility of the Helmholtz-Zentrum Berlin (BESSY II/HZB). Details about the system can be found elsewhere. [8,26]. The samples were palletized and pressed into a Cu mesh to reduce charging of the sample under X-ray beam. All samples were placed on a sapphire sample holder between a stainless steel backplate and a lid with 6 mm hole. Heating was done from the backside with an infrared laser. The sample temperature was measured with a K-type thermocouple positioned at the sample surface.

Au 4f spectra were acquired with the overall spectral resolution of 0.2 eV. The BE were calibrated using the Au $4f_{7/2}$ second order peak with accuracy of 0.05 eV. For quantitative XPS analysis, least-square fitting of the spectra was used (www.casaxps.com). . For deconvolution, a Doniach-Sunjic (DS) lineshape convoluted with a Gaussian function was used for Au $4f_{7/2}$.

$O_2$ and CO were dosed into the experimental cell using mass-flow controllers (MFC). Under reaction conditions the total pressure in the experimental cell was 0.3 mbar in flow mode.

TEM images were recorded using a Philips CEM 200 and a Cs-corrected (CEOS) FEI Titan 80-300 equipped with a Gatan Tridiem Image Filter.

CO oxidation was investigated in a plug-flow fixed-bed reactor at 1bar. Gases (He, $H_2$, $O_2$, CO) are mixed via custom-designed switching valves. The U-tube reactor (i.d. = 5mm) is made of glass lined steel and is connected to a four-way valve used as bypass. The reactor is heated by a copper block oven, providing an isothermal (±1 K) zone of 4 cm at temperatures up to 400 °C. The temperature is monitored inside the catalyst bed. Gas analytics are performed by an on-line detector consisting of IR detectors for CO, $CO_2$ and $H_2O$ and a paramagnetic sensor for $O_2$ (X-Stream, Rosemount).

DFT calculations were performed at the Perdew–Burke-Ernzerhof (PBE) level with the Quantum ESPRESSO [27] package using ultrasoft pseudopotentials from the PS Library [28] with a kinetic energy cutoff of 60 Ry and a charge density cutoff of 600 Ry. A **k**-point mesh equivalent to at

least 8x8 was used for the (110) surface unit cell of gold and Marzari-Vanderbilt cold smearing was employed with a smearing parameter of 0.02 Ry. Core level shift were computed using the ΔSCF method to capture both initial and final state effects [29]. The Au(110)/$TiO_2$(110) interface was modeled with a (1x11) 8-layer Au slab and (1x7) 3-layer rutile-$TiO_2$ cell to minimize lattice mismatch—the cells were doubled in the a direction, (2x11) and (2x7), when a core hole was included as part of the ΔSCF calculation. Periodic images were separated by *ca.* 10 Å of vacuum. The cell dimension were fixed to those of Au, requiring a 0.6% and 1.4% compression of $TiO_2$ in the (a,b) directions, respectively. The bottom (furthest from the interface) two layers of the Au slab were held fixed during geometry optimization. A 3-layer $TiO_2$ slab was chosen as there was a negligible difference in the core level shits computed a 2-layer or 3-layer $TiO_2$ slab. The work of adhesions was computed as the energy difference between Au/$TiO_2$ and the fully separated interface. The Au(110) surface energy was computed as the energy difference of a 21 atom slab, with the center 5 layers fixed, and bulk Au.

## Acknowledgements

We thank HZB for the allocation of synchrotron radiation beamtime. We gratefully acknowledge Höchstleistungsrechenzentrum Stuttgart (HLRS) for generous access to the supercomputer HazelHen. T. J. acknowledges the Alexander-von-Humboldt foundation for financial support.

**Keywords:** Gold nanoparticles • strong metal-support interaction • surface core-level shift • CO oxidation • ionic gold

[1] M. Haruta, N. Yamada, T. Kobayashi, S. Iijima, *J. Catal.* **1989**, *115*, 301-309.

[2] a) R. Meyer, C. Lemire, Sh. Shaikhutdinov, H.-J. Freund, *Gold Bull.* **2004**, *37*, 72-124; b) B. K. Min, C. M. Friend, *Chem. Rev.* **2007**, *107*, 2709-2724; c) G. J. Hutchings, J. K. Edwards in *Frontiers of Nanoscience, Vol. 3* (Eds.: L.J. Roy, J.P. Wilcoxon), Elsevier, Amsterdam, **2012**, pp. 249–293.

[3] a) C. K. Costello, J. H. Yang, H. Y. Law, Y. Wang, J.-N. Lin, L. D. Marks, M. C. Kung, H. H. Kung, *Appl. Catal. A* **2003**, *243*, 15-24; b) M. Valden, S. Pak, X. Lai, D. W. Goodman, *Catal. Lett.* **1998**, *56*, 7-10; c) M. Haruta, M. Daté, *Appl. Catal. A* **2001**, 222, 427–437; d) G. C. Bond, D. T. Thompson, *Gold Bull.* **2000**, *33*, 41–51.

[4] a) T. Minato, T. Susaki, S. Shiraki, H. S. Kato, M. Kawai, K. Aika, *Surf. Sci.* **2004**, 1012, 566–568; b) S. Laursen, S. Linic, *Phys. Rev. Lett.* **2006**, 97, 026101.

[5] a) M. P. Casaletto, A. Longo, A. Martorana, A. Prestianni, A. M. Venezia, *Surf. Interface Anal.* **2006**, 38, 215 – 218; b) J. Guzman B. C. Gates, *J. Am. Chem. Soc.* **2004**, 126, 2672-2673; c) L. Fu, N. Q. Wu, J.H. Yang, F. Qu, D. L. Johnson, M. C.Kung, H. H. Kung, V. P. Dravid, *J. Phys. Chem. B* **2005**, 109 , 3704-3706.

[6] A. Yu. Klyushin, Y. Youngmi, Z. Xie, R. Arrigo, M. Hävecker, A. V. Bukhtiyarov, I. P. Prosvirin, V. I. Bukhtiyarov, A. Knop-Gericke, R. Schlögl, *Top. Catal.* **2016**, *59*, 469-477.

[7] A. Yu. Klyushin, M. T. Greiner, X. Huang, T. Lunkenbein, X. Li, O. Timpe, M. Friedrich, M. Hävecker, A. Knop-Gericke, R. Schlögl, *ACS Catal.* **2016**, *6*, 3372-3380.

[8] M. Salmeron, R. Schlögl, *Surf. Sci. Rep.* **2008**, 63, 169-199; b) A. Knop-Gericke, E. Kleimenov, M. Hävecker, R. Blume, D. Teschner, S. Zafeiratos, R. Schlögl, V. I. Bukhtiyarov, V. V. Kaichev, I. P. Prosvirin, A. I. Nizovskii, H. Bluhm, A. Barinov, P. Dudin, M. Kiskinova, *Adv. Catal.* **2009**, *52*, 213-272.

[9] G. G. Fuentes, E. Elizalde, F. Yubero and J. M. Sanz, *Surf. Interf. Anal.* **2002**, *33*, 230-237.

[10] a) A. Yu. Klyushin, T. C. R Rocha, M. Hävecker, A. Knop-Gericke, R. Schlögl *Phys. Chem. Chem. Phys,* **2014**, *16*, 7881-7886; b) B. Koslowski, H.-G. Boyen, C. Wilderotter, G. Kästle, P. Ziemann, R. Wahrenberg, P. Oelhafen, *Surf. Sci.* **2001***, 475*, 1-10.

[11] a) J. Guzman, B. C. Gates, *J. Catal.* **2004**, 226, 111; b) A. Villa, N. Dimitratos, C. E. Chan-Thaw, C. Hammond, G. M. Veith, D. Wang, M. Manzoli, L. Prati, G. J.Hutchings, *Chem. Soc. Rev.* **2016**, 45, 4953–4994; c) J. C. Fierro-Gonzalez, V. A. Bhirud, B. C. Gates, *Chem. Commun.* **2005**, 42, 5275-5277.

[12] S. Laursen, S. Linic, *J. Phys. Chem. C* **2009**, *113*, 6689–6693.

[13] D. Widmann, R. J. Behm, *Angew. Chem. Int. Ed.* **2011**, *50*, 10241-10245.

[14] a) M. Haruta, *J. New. Mat. Electrochem. Systems* **2004**, *7*,163-172; b) B. E. Solsona, T. Garcia, C. Jones, S. H. Taylor, A. F. Carley, G. J. Hutchings, *Appl. Catal. A* **2006**, *312*, 67-76.

[15] a) S. J. Tauster, S. C. Fung, R. L. Garten, *J. Am. Chem. Soc.* **1978**, 100, 170-175; b) S. J. Tauster, S. C. Fung, *J. Catal.* **1978**, 55, 29-35; c) C. H. Bartholomew, R. B. Pannell, J. L. Butler, *J. Catal.* **1980**, 65, 335-347; d) C. C. Kao, S. C. Tsai, M. K. Bahl, Y. W. Chung, W. J. Lo, *Surf. Sci.* **1980**, 95, 1-14; e) M. A. Vannice, C. C. Twu, S. H. Moon, *J. Catal.* **1983**, 79, 70-80; f) M. A. Vannice, C. Sudhakar, *J. Phys. Chem. C* **1984**, 88, 2429-2432.

[16] D.Y. Cha, G. Parravano, *J. Catal.* **1970**, 18, 200-221.

[17] D. W. Goodman, *Cat. Let.* **2005**, 99, 1-4.

[18] C.C. Chusuei, X. Lai, K. Luo, D. W. Goodman, *Top. Cat.* **2001**, 14, 71-83.

[19] R. C. Baetzold, M. G. Mason, J. F. Hamilton, *J. Chem. Phys.* **1980**, 72, 366-368.

[20] W. F. Egelhoff, Jr., G. G. Tibbetts, *Solid State Commun.* **1979**, 29, 53-57.

[21] D. Widmann, A. Krautsieder, P. Walter, A. Bruckner, R. J. Behm, *ACS Catal.* **2016**, 6, 5005–5011.

[22] a) D. Widmann, D. R. Behm, *J. Acc. Chem. Res.* **2014**, 47, 740−749; b) B. W. Ewers, A. S. Crampton, M. M. Biener, C. M. Friend, *J. Phys. Chem. C* **2017**, 121, 21405–21410.

[23] a) Z. Duan, G. Henkelman, *ACS Catal.* **2015**, 5, 1589−1595. b) Z. Duan, G. Henkelman, *ACS Catal.* **2018**, 8, 1376−1383; c) Y.-G. Wang, D. C. Cantu, M.-S. Lee, J. Li, V.-A. Glezakou, R. Rousseau, *J. Am. Chem. Soc.* **2016**, 138, 10467−10476; d) L. Li, X. C. Zeng, *J. Am. Chem. Soc.* **2014**, 136, 15857−15860.

[24] M. Lohrenscheit, C. Hess, *ChemCatChem* **2016**, 8, 523-526.

[25] a) J. A. Rodriguez, G. Liu, T. Jirsak, J. Hrbek, Z. Chang, J. Dvorak, A. Maiti, *J. Am. Chem. Soc.* **2002**, 124, 5242-5250; b) N. Lopez, T. V. W. Janssens, B. S. Clausen, Y. Xu, M. Mavrikakis, T. Bligaard, J. K. Nørskov, *J. Catal.* **2004**, 223, 232-235; c) N. Lopez, J. K. Nørskov, T. V. W. Jannssens, A. Carlsson, A. Puig-Molina, B. S. Clausen, and J.-D. Grunwaldt, *J. Catal.* **2004**, 225, 86-94.

[26] H. Bluhm, M. Hävecker, A. Knop-Gericke, E. Kleimenov, R. Schlögl, D. Teschner, V. I. Bukhtiyarov, D. F. Ogletree, M. Salmeron, *J. Phys. Chem. B* **2004**, *108*, 14340-14347.

[27] P.Giannozzi, S. Baroni, N. Bonini, M. Calandra, R. Car, C. Cavazzoni, D. Ceresoli, G. L. Chiarotti, M. Cococcioni, I. Dabo, *J. Phys.: Condens. Matter* **2009**, *21*, 395502.

[28] A. D. Corso, *Comput. Mater. Sci.* **2014**, *95*, 337-350.

[29] E. Pehlke, M. Scheffler, *Phys. Rev. Lett.* **1993**, *71*, 2338-2341.

To address the question over the nature of Au activation we performed XPS measurements, DFT calculation, mass-spectroscopy and TEM. Our results show the formation of an ionic Au species during CO oxidation. DFT calculations show that oxidized $TiO_2$ and Au interact weakly, whereas reduced and defective $TiO_2$ show a strong metal-support interaction. Mass-spectroscopy confirms CO oxidation on supported Au via a Mars–van Krevelen like mechanism.

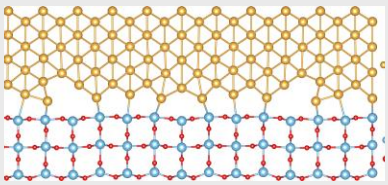

*Alexander Yu. Klyushin*, Travis E. Jones, Thomas Lunkenbein, Pierre Kube, Xuan Li, Michael Hävecker, Axel Knop-Gericke and Robert Schlögl*

***Page No. – Page No.***

**Strong Metal Support Interaction as a key factor of Au activation in CO oxidation.**